Coupled Atmosphere–Ocean Wave Simulations under High Wind Conditions

JAMES D. DOYLE

Naval Research Laboratory, Monterey, California

(Manuscript received 14 September 2001, in final form 31 May 2002)

ABSTRACT

The impact of ocean surface waves on the structure and intensity of three tropical cyclones and a topographically forced bora event is investigated using a coupled atmosphere–ocean wave modeling system. The coupled system is capable of representing surface momentum fluxes that are enhanced due to young ocean waves in fetch-limited conditions, which yield surface roughness lengths that significantly depart from the conventional Charnock-type formulation. In general, the impact of ocean-wave-induced stress on the tropical cyclone central pressure was quite variable with ocean wave feedback resulting in changes ranging from 8 hPa deeper to 3 hPa shallower. The increased low-level stress due to the ocean waves reduced the near-surface winds by 2–3 m s^{-1}, with local differences in excess of 10 m s^{-1}, which directly led to a 10% reduction in the significant wave height maxima. The reduced significant wave heights in the coupled model were in closer agreement with observations for Tropical Cyclone Bonnie than for the uncoupled model. The tropical cyclone tracks were generally insensitive to ocean wave feedback effects. The boundary layer structure was found to be generally insensitive to large roughness enhancements associated with coupled ocean wave feedbacks for topographically forced high wind phenomena, such as the bora.

1. Introduction

The exchange of heat, momentum, and moisture between the air and sea has long been recognized as a fundamental process in the development of a number of mesoscale atmospheric phenomena such as tropical cyclones, extratropical cyclones, boundary layer jets, coastal fronts, and precipitating systems. Numerical prediction of these phenomena is often critically dependent on the fidelity of surface flux representation (e.g., Emanuel 1995). This air–sea exchange takes place at the fluid interface in the wave boundary layer, which underscores the potential importance of ocean surface waves in air–sea interaction processes.

Ocean surface gravity waves can have a significant impact on the interaction between the atmosphere and ocean through modulation of the transfer of momentum and enthalpy across the air–sea interface (e.g., Donelan 1990). As air flows over the sea, wind stress contributes to both the generation of surface gravity waves and the forcing of local ocean currents and circulations. The conventional representation of the surface roughness effects over the sea due to ocean waves, based on the scaling arguments of Charnock (1955), is used by nearly all atmospheric research and operational models, and is strictly valid only for fully developed ocean wave conditions. Under high wind conditions, however, wind direction and speed are often time dependent, such as for a translating tropical cyclone or topographically driven flows in the coastal zone. In these fetch-limited conditions, surface ocean waves have an increasingly important impact on the momentum flux in the atmospheric and oceanic boundary layers (Donelan 1990). In situations when the wave age is small, the wave-induced stress composes a significant fraction of the total stress. A number of previous studies using field measurements have documented this dependence of the atmospheric momentum flux on the ocean wave age (e.g., Smith et al. 1992). It should be noted that experimental and theoretical evidence suggests that although a sea state dependence exists for the surface momentum flux, no similar dependence has been suggested for heat and moisture fluxes (Geernaert et al. 1987). The interaction between the sea and air is especially complex at high wind speeds where flux exchange processes may be impacted by sea spray and spume (Kepert et al. 1999; Wang et al. 2001) and airflow separation due to breaking surface waves (Kudryavtsev and Makin 2001).

Wave-induced stress may be a significant component of the total momentum stress in the atmospheric boundary layer over the ocean (e.g., Donelan 1990; Janssen 1991) and has been suggested to enhance the decay of extratropical systems on the mesoscale (e.g., Doyle 1995; Desjardins et al. 2000), impact the wave prediction in extreme sea states associated with midlatitude cyclones (Lalbeharry et al. 2000), and modulate the ex-

Corresponding author address: James D. Doyle, Naval Research Laboratory, Marine Meteorology Division, 7 Grace Hopper Ave., Monterey, CA 93943-5502.
E-mail: doyle@nrlmry.navy.mil

Report Documentation Page

Form Approved
OMB No. 0704-0188

1. REPORT DATE	2. REPORT TYPE	3. DATES COVERED
31 MAY 2002		**00-00-2002 to 00-00-2002**

4. TITLE AND SUBTITLE	5a. CONTRACT NUMBER
Coupled Atmosphere-Ocean Wave Simulations under High Wind Conditions	5b. GRANT NUMBER
	5c. PROGRAM ELEMENT NUMBER
6. AUTHOR(S)	5d. PROJECT NUMBER
	5e. TASK NUMBER
	5f. WORK UNIT NUMBER
7. PERFORMING ORGANIZATION NAME(S) AND ADDRESS(ES) **Naval Research Laboratory,7 Grace Hopper Ave., Stop 2 ,Monterey,CA,93943-5502**	8. PERFORMING ORGANIZATION REPORT NUMBER
9. SPONSORING/MONITORING AGENCY NAME(S) AND ADDRESS(ES)	10. SPONSOR/MONITOR'S ACRONYM(S)
	11. SPONSOR/MONITOR'S REPORT NUMBER(S)

12. DISTRIBUTION/AVAILABILITY STATEMENT
Approved for public release; distribution unlimited

13. SUPPLEMENTARY NOTES

14. ABSTRACT
see report

15. SUBJECT TERMS

16. SECURITY CLASSIFICATION OF:			17. LIMITATION OF ABSTRACT	18. NUMBER OF PAGES	19a. NAME OF RESPONSIBLE PERSON
a. REPORT **unclassified**	b. ABSTRACT **unclassified**	c. THIS PAGE **unclassified**	**Same as Report (SAR)**	**13**	

tratropical storm track (Weber et al. 1993; Janssen and Viterbo 1996). Zhang and Perrie (2001) found that heat and moisture fluxes dominate momentum feedbacks due to wave effects behind cold fronts in extratropical cyclones, while momentum fluxes appear to be more important ahead of and near the cyclone center. Powers and Stoelinga (2000) applied a coupled air–sea model to Lake Erie and noted that roughness enhancement due to wave age effects modulated the local planetary boundary layer and downstream flow. The impact of wind-generated ocean waves on the structure and evolution of mesoscale phenomena that are primarily forced by (i) air–sea fluxes such as tropical cyclones and (ii) coastal orography have received considerably less attention. This study describes a series of numerical simulations using the Naval Research Laboratory's (NRL) Coupled Ocean–Atmosphere Mesoscale Prediction System (COAMPS) coupled with the Wave Model (WAM) to evaluate the impact of air–sea interaction on the development and track of tropical cyclones and the evolution of topographically forced flows in the coastal zone. Although we recognize that the ocean mixed layer and sea spray may be important components of the air–sea interaction processes (e.g., Bao et al. 2000), in this study we focus only on interaction of sea surface waves and the atmosphere as a first step toward fully modeling the air–sea interaction system. The numerical model is described in section 2. The results of the coupled simulations are presented in section 3, followed by the summary and conclusions in section 4.

2. Numerical model description

The atmospheric model used in this study is NRL's COAMPS (Hodur 1997; Hodur and Doyle 1999). Finite-difference approximations are used in the model to represent the fully compressible, nonhydrostatic equations that govern atmospheric motions. The equations are solved in three dimensions, with a nested-grid mesh capability, using a terrain-following vertical coordinate transformation. The finite-difference schemes are of second-order accuracy in time and space. The compressible equations are integrated efficiently through the use of a time-splitting technique that features a semi-implicit treatment in the vertical for the acoustic modes.

A prognostic equation for the turbulent kinetic energy (TKE), e, budget is used to parameterize the planetary boundary layer and free-atmospheric turbulent mixing and diffusion based on the level 2.5 formulation of Mellor and Yamada (1982) as follows:

$$\frac{\partial e}{\partial t} = -u\frac{\partial e}{\partial x} - v\frac{\partial e}{\partial y} - \dot{\sigma}\frac{\partial e}{\partial \sigma} + \mathrm{BP} + \mathrm{SP} + D - \varepsilon, \quad (1)$$

where u and v are the horizontal wind velocity components, BP is the buoyancy production, SP is the shear production, D is the subgrid-scale vertical mixing of TKE, and ε is the dissipation rate. The eddy diffusivity coefficients for heat and momentum are directly proportional to $e^{1/2}$. The surface fluxes are computed following the Louis et al. (1982) formulation, which is an approximation to Monin–Obukhov similarity theory. In the standard application of COAMPS when a predictive ocean wave model is not used in a tightly coupled manner, z_0 is represented over the open sea by the Charnock relationship (Charnock 1955):

$$z_0 = \alpha\frac{\tau}{g\rho}, \quad (2)$$

where τ is the magnitude of the turbulent stress, ρ is the density, and α is the Charnock parameter taken to be 0.0185.

A force–restore method is used to parameterize the land surface energy budget. Parameterization of short- and longwave radiation processes, and subgrid-scale moist convective processes, are included as well. Budget equations for cloud water, cloud ice, raindrops, snowflakes, and water vapor are used to represent the grid-scale evolution of the moist processes. For more details of the parameterization methodology, see Hodur (1997) and Hodur and Doyle (1999).

Multivariate optimum interpolation analysis of upper-air sounding, surface, aircraft (automated weather reports from commercial aircraft; ACARS) and satellite data that are quality controlled is the basis for the initial state of the nonhydrostatic model. The Navy Operational Global Analysis and Prediction System (NOGAPS) forecast fields are used for lateral boundary conditions. The application of COAMPS in this type of manner closely emulates a real-time numerical prediction system in spite of the simulations being performed in a hindcast mode. The atmospheric topographic data are based on the U.S. Defense Mapping Agency's 100-m resolution dataset.

The atmospheric model is coupled in an interactive mode to the third generation (cycle 4) of the WAM (WAMDI Group 1988). The quasi-linear theory of wind-wave generation following Janssen (1989) and Janssen (1991) is applied. The transport equation is integrated to solve for the wave variance spectrum for 25 frequencies and 24 directions. The processes represented in WAM include wind–wave interaction, transfer of energy within the wave spectrum, wave propagation, and dissipation by whitecapping.

The coupling methodology follows Janssen (1989) and Janssen (1991) and includes the processes represented by mutual interaction of the wind waves and boundary layer stress. The roughness length used in the coupled simulation is represented by

$$z_0 = \beta\frac{\tau}{g\rho(1 - \tau_w/\tau)^{0.5}}, \quad (3)$$

where τ is the total stress and τ_w is the wave-induced stress. The constant β is chosen as 0.01 implying that (3) reduces to the standard Charnock relationship (2) for a saturated wave state ($\tau_w = 0$). The wave-induced

stress is primarily determined by the high frequency portion of the spectrum because these waves have the fastest growth rate due to the wind forcing (Janssen 1989). For a young wind sea, it follows that the effective Charnock parameter can be enhanced by an order of magnitude. The simultaneous coupling is physically achieved through communicating the 10-m wind speed to the wave model every WAM time step. An iterative technique is then used to calculate τ_w based on the wind speed, drag coefficient, and stress. The new wave-induced Charnock parameter is subsequently used in the Louis et al. (1982) flux calculations in the atmospheric model. This coupling technique using the WAM and an atmospheric model has been applied previously to study air–sea interaction in extratropical cyclones (e.g., Doyle 1995; Lionello et al. 1998; Desjardins et al. 2000; Lalbeharry et al. 2000) and tropical cyclones (Bao et al. 2000). The coupling technique using the WAM is currently being applied operationally at the European Centre for Medium-Range Weather Forecasts (ECMWF) and the results indicate a substantial positive impact on the skill of the atmosphere and ocean wave model forecasts (Janssen et al. 2002). Desjardins et al. (2000) showed that an empirical sea-state-dependent z_0, based on data collected during the Humidity Exchange Over the Sea (HEXOS) experiment, yields consistent results with (3). In this study, the uncoupled simulations are performed with simultaneous integration of the WAM except the standard Charnock parameter of 0.0185 is used in the atmospheric model flux calculations.

3. Coupled simulations

To isolate the importance of the wave coupling, two experiments are performed for each case. The first simulation makes use of the conventional Charnock parameter in the atmosphere and includes a wave simulation based on the atmospheric winds every WAM time step. The second simulation includes the wave-induced stress effects in the modified Charnock formulation following (3) and also includes the feedback of the atmospheric winds, already modified by wave-induced roughness, back to the waves.

Coupled and uncoupled COAMPS/WAM simulations were performed for Tropical Cyclones Bonnie, Mitch, and Bret, and a topographically forced high wind event. A horizontal grid dimension of 133 $\times$ 133 with an increment of 12 km was used for both COAMPS and WAM model simulations of Tropical Cyclones Mitch and Bret. Two nested grids were used for the simulations of Bonnie. A fine mesh grid of 181 $\times$ 181 points and an increment of 6 km were used with an identical grid domain and resolution for the single WAM mesh. The coarse mesh for the atmospheric model contained 133 $\times$ 133 points with a resolution of 18 km. The simulation of the topographically forced wind event made use of a single mesh with 133 $\times$ 133 points and a horizontal grid increment of 5 km. Thirty vertical levels were used in the atmospheric model with a top at 34 km and a lowest model level at 10 m above ground. A terrain-following vertical coordinate is used that features horizontal model surfaces over water and flat land (Hodur 1997). In the WAM, the wave spectrum is discretized using 24 directions and 25 frequencies in the range 0.033–0.33 Hz for all experiments. The directional discretization is rotated by 7.5° to avoid a systematic bias in the energy propagation.

a. Tropical Cyclone Bonnie simulations

Tropical Cyclone Bonnie strengthened to hurricane force at 0600 UTC 22 August 1998 when it was located 400 km north of Hispaniola. Bonnie moved on a general west-northwest heading reaching maximum strength of 51 m s^{-1} and a central pressure of 954 hPa. Eventually, Bonnie made landfall near Wilmington, North Carolina, at approximately 0330 UTC 27 August. The time period of interest in this study is during an earlier phase of the tropical cyclone on 24 August. On this day, the sea surface directional wave spectrum was measured using the National Aeronautics and Space Administration (NASA) airborne Scanning Radar Altimeter (SRA) carried aboard a National Oceanic and Atmospheric Administration (NOAA) WP-3D hurricane research aircraft at a height of 1.5 km (Wright et al. 2001). A description of the instrument, error characteristics, and applications can be found in Walsh et al. (1996) and Wright et al. (2001).

The Charnock parameter for 1200 UTC 24 August 1998 (24-h simulation time) for the coupled simulation, shown in Fig. 1a, indicates a large region of enhanced Charnock parameter outside the tropical cyclone eye. The northern or right-of-track half of the tropical cyclone contains the region with the largest wave-induced stress, resulting in Charnock parameter maxima in excess of 0.09. The wave age parameter, C_p/u_* where C_p is the phase speed of the peak spectral frequency and u_* is the friction velocity, for 1200 UTC 24 August, is shown in Fig. 1b. The wave age is consistent with the Charnock parameter distribution and indicates that the youngest ocean waves are located in the northern half, with swell dominating the eye and outer regions of the tropical cyclone. Clearly in these tropical cyclone situations, the strong curvature of the wind field limits the fetch. As a result of the fetch-limited conditions, the roughness length was enhanced substantially from values of 10^{-5} m present in the near-calm regions within the eye and outside of the tropical cyclone, to greater than 0.03 m in the northeastern quadrant (Fig. 1c).

Typically, the wind speed in a tropical cyclone is largest in the region that contains winds with the same direction as the storm motion because the forward translation speed of the storm contributes to higher speeds. In this region, the waves propagate in the direction of the storm motion so that a given wave packet may be under the influence of a consistent wind direction and

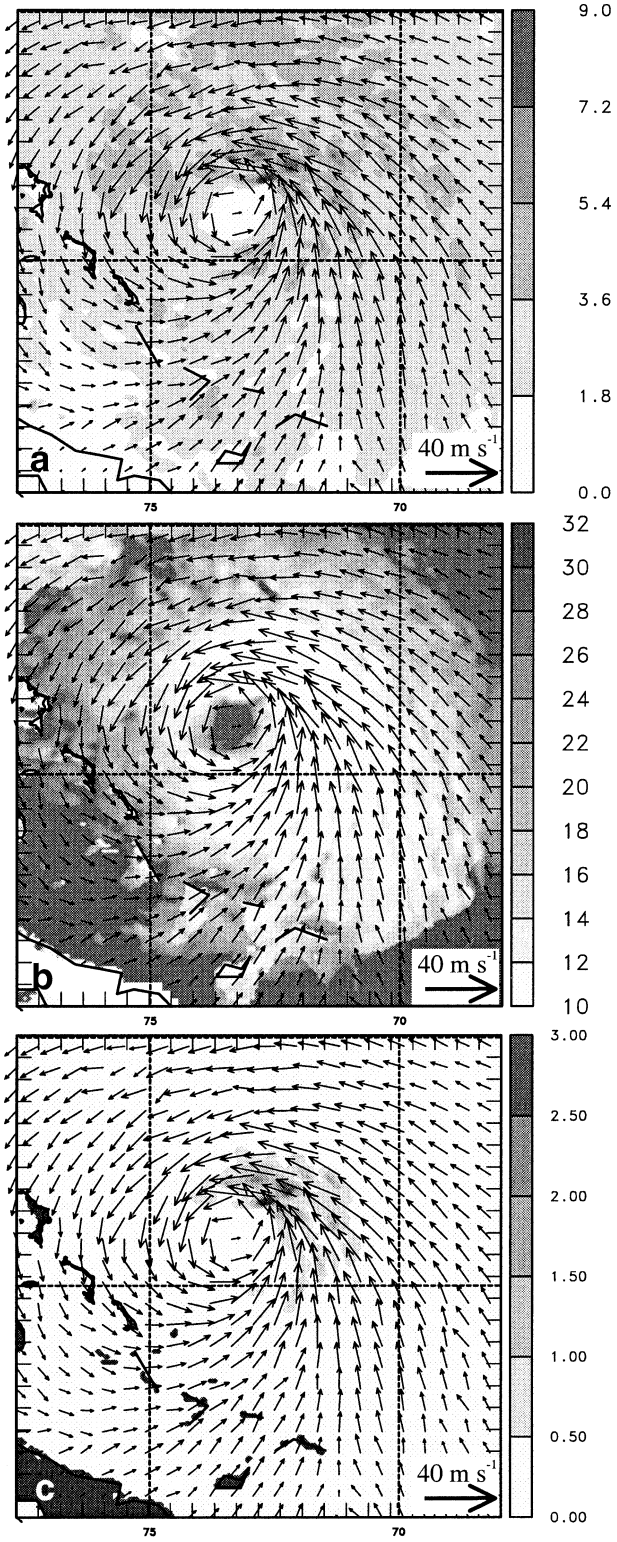

FIG. 1. Coupled simulation for 1200 UTC 24 Aug 1998 of (a) nondimensional Charnock parameter ($\times 10^{-2}$), (b) wave age, and (c) roughness length ($\times 10^{-2}$ m). Winds at 10 m are indicated by the vectors.

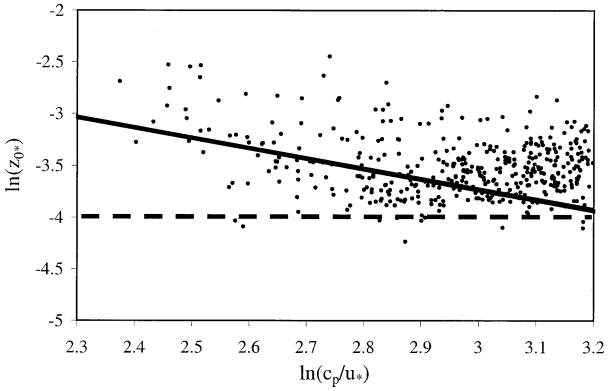

FIG. 2. Simulated dimensionless roughness length ($z_{0^*} = gz_0/u_*^2$) as a function of the wave age for the coupled simulation at 1200 UTC 24 Aug. The Charnock parameter of 0.0185 is shown by the dashed line at $\ln(z_{0^*}) = -4.0$. The solid line represents the Smith et al. (1992) best fit.

speed for a longer period and distance (Wright et al. 2001). These resonance processes act to increase the fetch and duration in the same direction as the storm motion (Young 1988; MacAfee and Bowyer 2000), particularly when the group velocity of the waves and translation speed of the tropical cyclone are comparable (Moon et al. 2002). These factors along with the fetch-limited effects due to curvature in the wind field result in an enhanced wave-induced surface roughness in the right half of the tropical cyclone. Additionally, the asymmetry in the storm-scale structure, with the greatest precipitation and cloud shield located in the northern half, as indicated by satellite imagery, may also have influenced the asymmetric wave state characteristics.

The relationship between the simulated wave age parameter and the dimensionless roughness length (gz_0/u_*^2) for 1200 UTC 24 August is shown in Fig. 2. Model-simulated data extracted from every fifth grid point over the entire domain are displayed. The regression fit based on observational data from Smith et al. (1992) taken during HEXOS, shown in Fig. 2, indicates a reasonable agreement between the observations and simulated wave age and Charnock parameters, as is also discussed in the coupled model results of Janssen et al. (2002). In this case of extreme winds the young waves in the range from approximately 2.3 to 3.0 appear to have a larger negative slope than the Smith et al. (1992) data would indicate. The larger negative slope exhibited by this distribution is in agreement with the wave-age-dependent Charnock parameters computed by Oost et al. (2001) based on eddy correlation measurements in the North Sea. The uncoupled simulations, which do not feedback the wave-induced stress, use a dimensionless roughness length of -4.0 or $\alpha = 0.0185$ over the water. A constant Charnock parameter of 0.0185 is sufficiently accurate for a fully saturated wave state ($C_p/u_* > 25$). However, for a relatively young wind sea ($C_p/u_* < 25$), the use of the standard Charnock value significantly underestimates the dimensionless roughness (e.g., Smith

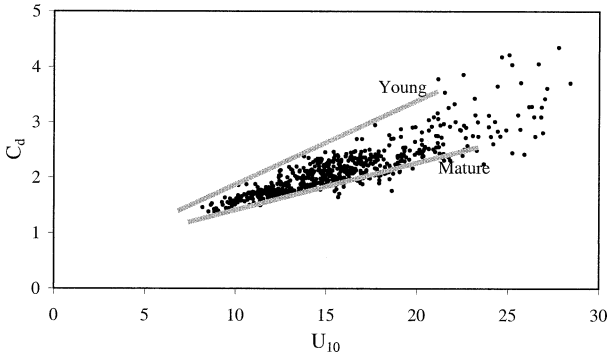

FIG. 3. Neutral drag coefficient ($\times 10^{-3}$) as a function of wind speed from the coupled simulation at 1200 UTC 24 Aug. Gray-shaded lines indicate drag coefficients associated with very young and fully developed wave states following Smith et al. (1992).

et al. 1992). It follows that young waves will be associated with a larger effective drag coefficient than for a fully developed wave state (e.g., Geernaert et al. 1987), as illustrated in Fig. 3. Thus, the differences between the uncoupled and coupled simulations can be attributed to the roughness enhancement due to young ocean waves. It should be noted that in this simulation the dimensionless roughness exceeds the Charnock value for fully developed waves at a number of points in general agreement with the Oost et al. (2001) North Sea measurements. This may not be unexpected given the complex wave state that dominates nearly the entire inner-mesh domain. Applications of the coupled model using this parameterization to other cases such as extratropical cyclones, which contain weaker wind speeds, indicate a closer agreement with the Smith et al. (1992) regression curve for the fully developed regime (e.g., see Fig. 4 in Doyle 1995).

Relevant aspects of the Bonnie simulation for 1200 UTC 24 August (24-h simulation time) and 0000 25 August (36-h simulation time) are summarized in Table 1. The central pressures for the coupled and uncoupled simulations are quite similar and within 2 hPa of each other, a result also noted by Desjardins et al. (2000) for extratropical cyclones. However, the observed central pressure is 15–20 hPa deeper than simulated in the coupled and uncoupled simulations. The tropical cyclone track is nearly identical between the coupled and uncoupled simulations. Similar maximum horizontal velocities at 10 m and 500 m are attained in the two simulations.

The most substantial differences between the simulations are apparent in the significant wave height fields. The coupled simulation has a significant wave height maximum that is reduced by approximately 15% relative to the uncoupled case. Both the coupled and uncoupled simulations make use of new atmospheric winds every wave model time step. The SRA-derived significant wave height and dominant wavelength superimposed on the NOAA's Atlantic Oceanographic and Meteorological Laboratory/Hurricane Research Division (AOML/HRD) surface wind field analysis are shown in Fig. 4 (from Wright 2000). The maximum significant wave height derived from this composite analysis of five flight segments is approximately 10.5 m. It is noteworthy that the dominant waves propagate at significant angles to the low-level wind direction. The significant wave height maximum is located in the northeast quadrant (Fig. 4a) where the field is dominated by swell (Fig. 4b). In the southern half of the tropical cyclone, the dominant wavelength is considerably shorter relative to the long wavelength associated with the swell located in the northern half.

The simulated significant wave heights for the uncoupled and coupled simulations of Tropical Cyclone Bonnie are shown in Fig. 5. As noted above, the significant wave height maximum in the northeastern quadrant is considerably reduced in the coupled simulation, in spite of the dominance of the swell. The coupled simulation is in overall closer agreement with the SRA-derived wave field than the uncoupled case. Lalbeharry et al. (2000) also found that two-way coupling has some positive impact through the mitigation of the overprediction of significant wave height maxima apparent in uncoupled simulations, particularly in cases with extreme sea states as considered here. The dominant wavelength is shown in Fig. 6 for the uncoupled and coupled simulations. Considering the complexity of both the wave and wind fields, the simulated wavelength contains many common characteristics with the SRA composite wavelength field (Fig. 4b) including the dominance of

TABLE 1. Summary of the simulated central pressure (SLP), wind speed maximum (U_{max}), significant wave height maximum (H_s), and maximum Charnock parameter value (α_{max}) for Tropical Cyclone Bonnie valid at 1200 UTC 24 Aug (24 h) and 0000 UTC 25 Aug 1998 (36 h). Observed estimates from the best track are shown as well. The uncoupled and coupled wind speed maxima are shown for the 10- and 500-m levels, respectively.

Variable	Simulation time (h)	Uncoupled	Coupled	Observed
SLP	24	982.6 hPa	983.2 hPa	962 hPa
SLP	36	980.2 hPa	978.7 hPa	964 hPa
U_{max}	24	35.4/54.1 m s^{-1}	32.1/52.2 m s^{-1}	51.0 m s^{-1}
U_{max}	36	33.4/49.7 m s^{-1}	35.1/54.7 m s^{-1}	51.0 m s^{-1}
H_s	24	12.8 m	10.9 m	10.5 m
H_s	36	12.6 m	11.0 m	
α_{max}	24	0.0185	0.15	
α_{max}	36	0.0185	0.11	

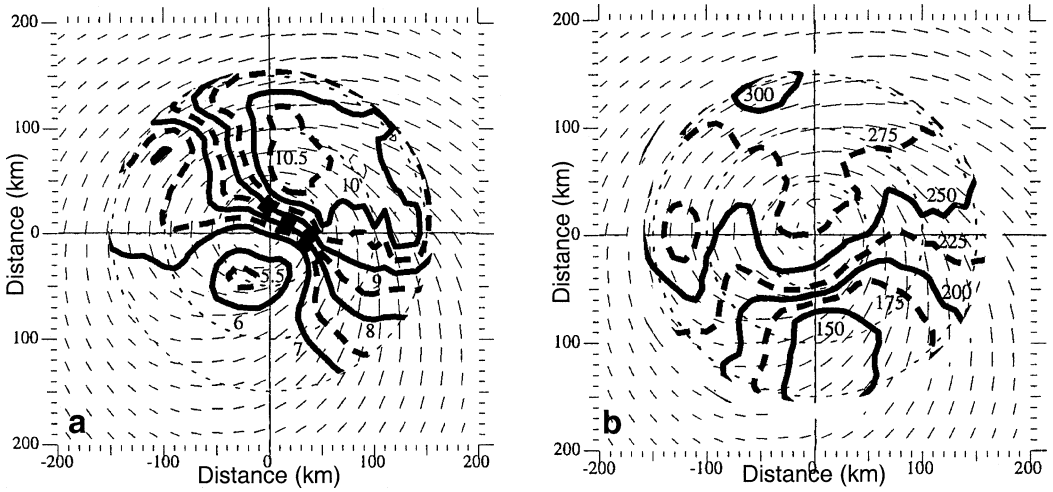

FIG. 4. NASA airborne SRA-derived (a) significant wave height (m) and (b) dominant wavelength (m) based on NOAA WP-3D research aircraft data from 24 Aug 1998 (modified from Wright 2000 and Wright et al. 2001).

swell in the northern half and shorter wavelengths in the southern portion of the tropical cyclone. The dominant wavelength in the coupled simulation (Fig. 6b) is slightly shorter in the northern half of the tropical cyclone than the uncoupled simulation (Fig. 6a). Both the coupled and uncoupled simulations contain a region south of the eye characterized by wavelengths less than 100 m, whereas the SRA observations indicate slightly longer wavelengths greater than 150 m. The SRA measurements indicate that the swell propagated in a northwesterly direction aligned with the track of the tropical cyclone. Wright et al. (2001) hypothesized that the dominance of the northwesterly swell was due to higher wind speeds and wave resonance effects that increased the effective fetch, which occurred in the northern half of the tropical cyclone. The coupled and uncoupled simulations both capture the many characteristics of the SRA directional wave spectra, such as the dominance of northwesterly propagating swell and the tendency for multiple modes in the southeastern quadrant. It is noteworthy, however, that the radial distance from the tropical cyclone eye to the wave height maximum was observed to be approximately 70 km based on the SRA data and 200 km in the model simulation. Although the coupled simulation appears to be in general agreement with a number of observed features and characteristics, fundamental deficiencies in the model simulation of the tropical storm structure and intensity clearly exist.

The directional wave spectra as measured from the SRA, shown in Fig. 7 (from Wright et al. 2001), illustrate a number of complex characteristics of the wave field. At several locations wave spectra were extracted from the coupled simulation for similar regions as the SRA observations (Fig. 7a) and are shown in Fig. 8 (in eye-relative coordinates). In the northwestern quadrant at location point 1, the observed (Fig. 7b) and simulated (Fig. 8a) directional wave spectra contain common characteristics including a westward propagating swell with

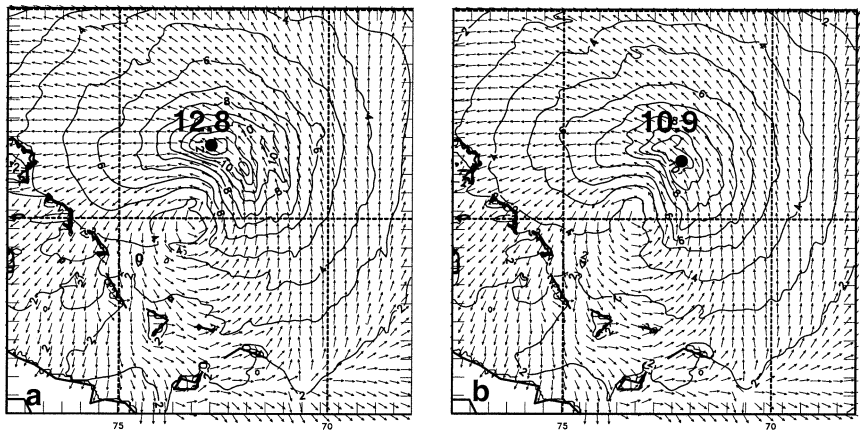

FIG. 5. Simulated significant wave height (m) and direction (vectors) for the (a) uncoupled and (b) coupled simulations valid at 1200 UTC 24 Aug 1998 (24 h).

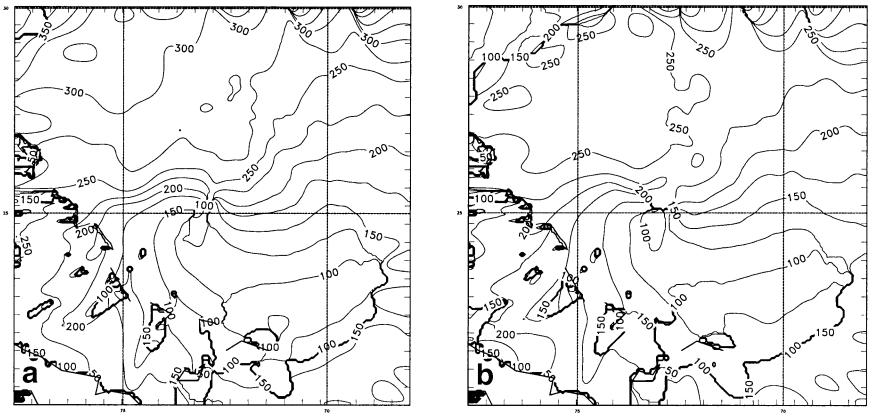

FIG. 6. Wavelength (m) of the wave spectrum peak valid at 1200 UTC 24 Aug 1998 (24 h) for the (a) uncoupled and (b) coupled models.

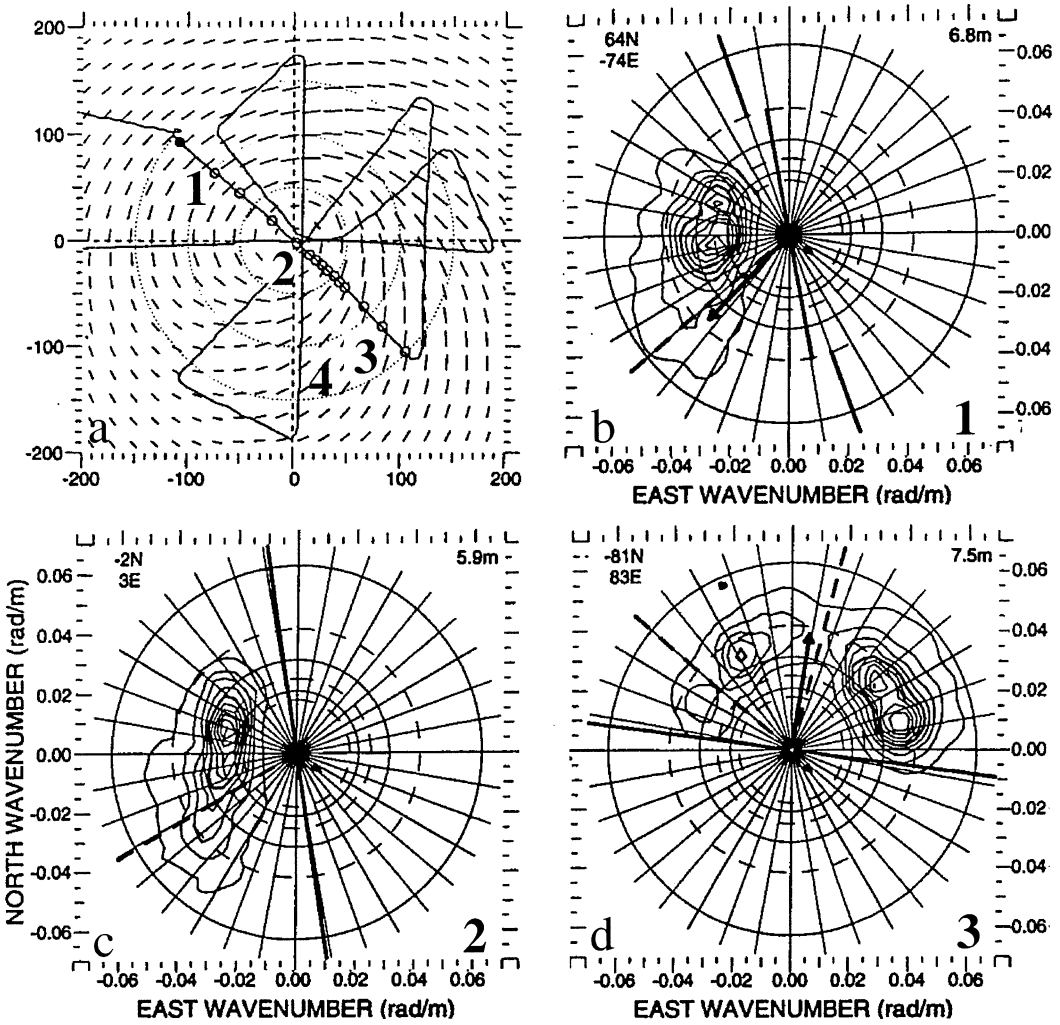

FIG. 7. Observed directional wavenumber spectra from the NASA SRA measured between 2030 and 2115 UTC 24 Aug 1998. (top-left) The NOAA aircraft track and HRD surface winds field (speed of 30 m s^{-1} corresponds to a length of 10 km) and the location of the spectra of interest relative to the tropical cyclone center (modified from Wright et al. 2001). The outer solid circle in each spectrum corresponds to 100 m, and the inner circles represent wavelengths of 150, 200, 250, 300, and 350 m.

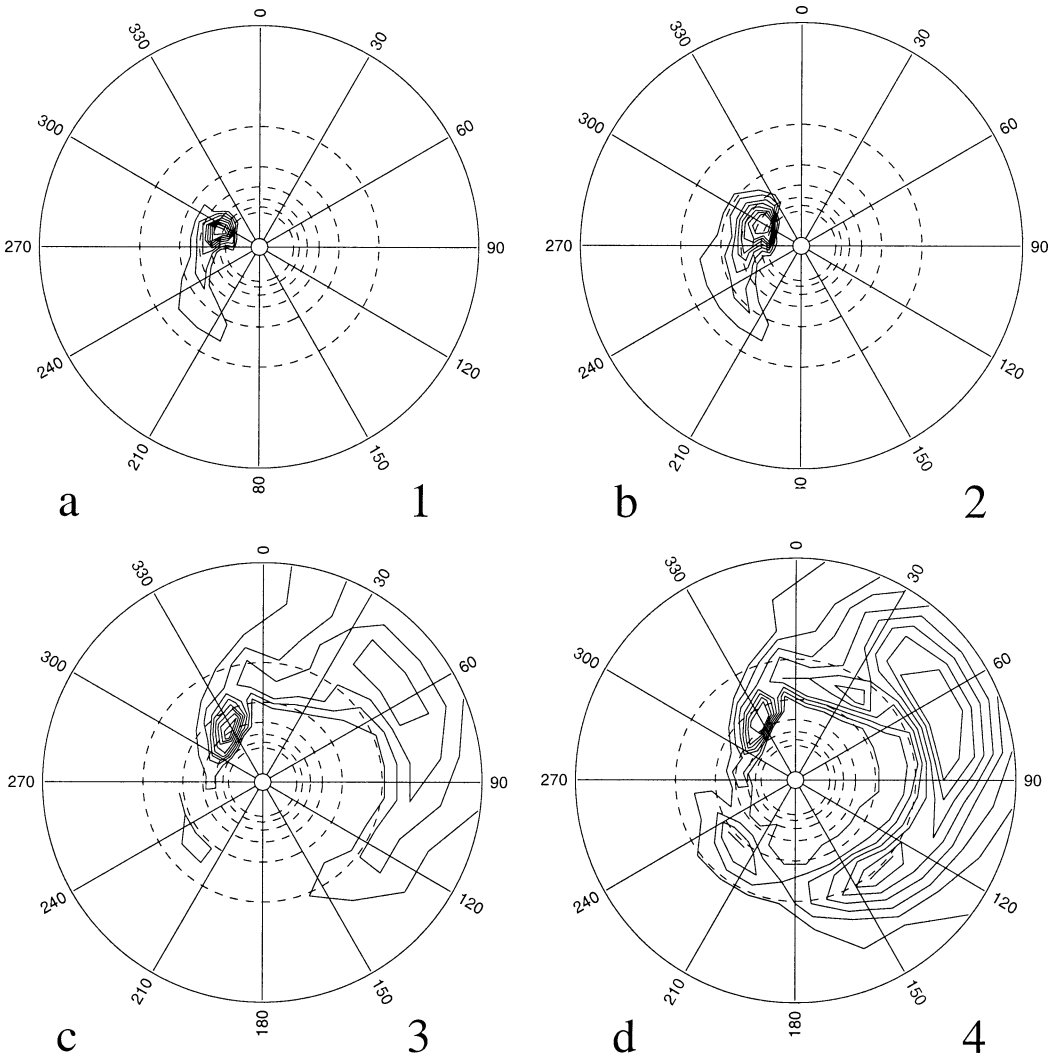

FIG. 8. Simulated directional wave spectra from the coupled simulation valid at 1200 UTC 24 August 1998. The solid outer circle corresponds to the 50-m wavelength. The dashed circles indicate the 100-, 150-, 200-, 250-, 300-, and 350-m wavelengths. The spectra are individually normalized. The locations correspond to the relative positions to the tropical cyclone as shown in Fig. 7a and are denoted by the number in the lower right.

wind-generated waves manifested as a tail on the spectrum that extends toward shorter wavelengths or higher frequencies. The model-simulated peak in the energy spectrum occurs near 275 m, which is a slightly longer wavelength than the observed peak at 250 m. Near the tropical cyclone eye at location point 2, the observed (Fig. 7c) and simulated (Fig. 8b) spectra both contain a similar signature with westward propagating swell. The wavelength at the peak of the spectrum, 275 m, is once again slightly longer than the derived value from the SRA, 250 m. In the southeastern quadrant at location point 3, the observed (Fig. 7d) and simulated (Fig. 8c) spectra indicate a bimodal wave field with a northeast propagating wind-generated sea superimposed on a northwest propagating swell. However, at location 3, the SRA-observed wave state is characterized by greater energy and longer wavelengths in the northeast propagating waves than the coupled simulation indicated. This difference may arise from the deficiencies in the atmospheric model simulation of the tropical cyclone structure. An additional point extracted south of the cyclone eye, at location 4, indicates an even more complex wave state with multiple wind sea modes coincident with a northwest propagating swell. Although the identical frequency spectrum was not sampled by the SRA at this point, a number of complex trimodal wave spectra were noted in the vicinity by Wright et al. (2001). Overall, wave spectra from the uncoupled simulation tended to contain qualitatively similar structures as the fully coupled model with much greater differences in the wave spectra between the quadrants surrounding the tropical cyclone than the differences between the two simulations.

Although significant quantitative differences exist in

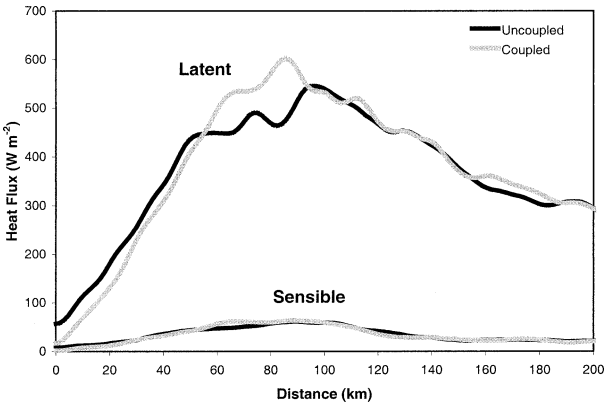

FIG. 9. Radial distribution of the azimuthally averaged sensible and latent heat fluxes for the simulation of Tropical Cyclone Bonnie valid at 1200 UTC 24 Aug (24 h). The uncoupled and coupled simulation results are denoted by the dark and gray curves, respectively.

the wave properties between the uncoupled and coupled simulations, the surface heat fluxes are quite similar between the two experiments. The radial distribution of the sensible and latent heat flux averaged azimuthally at the surface is shown in Fig. 9 for 1200 UTC 24 August 1998 (24 h). The averaged latent heat flux in the coupled simulation is approximately 10%–20% larger than the uncoupled experiment at radial distances of 50–100 km from the cyclone center. The enhanced surface moisture heat flux is a direct result of the increased stress associated with young ocean waves and the corresponding augmented Charnock parameter. However, surface flux parameterizations commonly applied in atmospheric models such as COAMPS are not designed for the high wind speed regime and it follows that considerable uncertainties exist in the air–sea flux representation.

b. Tropical Cyclone Mitch simulations

The observed minimum central pressure in Tropical Cyclone Mitch was estimated to be 905 hPa with sustained surface wind speed in excess of 80 m s^{-1}, distinguishing Mitch as the strongest October hurricane in the Atlantic basin on record. Tropical Cyclone Mitch was responsible for over 9000 deaths, making it one of the deadliest Atlantic tropical cyclones in history.

The simulated central pressure, 10- and 500-m wind speed maxima, maximum significant wave height, and maximum Charnock parameter for 0000 UTC 26 October (24-h simulation time) and 0000 UTC 27 October (48-h simulation time) 1998 are summarized in Table 2. The central pressure is approximately 8 hPa lower in the coupled simulation than in the uncoupled case at the 48-h time. As a result of the enhanced surface stress, the momentum flux increases considerably due to the coupled response. In the parameterization of the surface fluxes, the heat and moisture fluxes are influenced by the wave state through the surface momentum flux. For example, at 0000 UTC 27 October wave-induced effects increase the maximum surface sensible heat flux by nearly a factor of 2, from a maximum of 506 to 946 W m^{-2}. However, uncertainties clearly exist in the surface flux parameterization in this environment. The azimuthally averaged latent heat flux nearly doubles from 1500 W m^{-2} in the uncoupled experiment to 2900 W m^{-2} in the coupled simulation at a radial distance of 24 km. This increase in the heat flux contributes to a 30% increase in the azimuthally averaged rainfall that leads to an 8-hPa reduction in central pressure in the coupled simulation. However, because of the increased drag due to the young ocean waves, the maximum wind speed below 500 m is less for the coupled simulation. A second coupled simulation was performed using the surface heat and moisture flux computed using a surface stress based on the Charnock parameter and independent of wave age. The simulated minimum pressure was 941.4 hPa for this coupled simulation, which is 8 hPa higher than the uncoupled simulation and 16 hPa greater than the coupled simulation with the heat and moisture fluxes dependent on the wave state. Clearly, the heat and moisture exchange coefficients appear to have a very important effect on tropical cyclone intensity relative to momentum flux changes due to wave-induced stress, a similar conclusion to that noted by Zhang and Perrie (2001) for an extratropical cyclone.

As a result of weaker surface winds due to enhanced roughness associated with the young ocean waves, the significant wave height maximum is 2 m less in the coupled simulation, as shown in Table 2 and Fig. 10 for 0000 UTC 27 October. The increased stress associated with the young ocean waves does not appear to have a

TABLE 2. Same as Table 1, except for Tropical Cyclone Mitch valid at 0000 UTC 26 Oct (24 h) and 0000 UTC 27 Oct 1998 (48 h). Observed estimates from the best track are shown as well.

Variable	Simulation time (h)	Uncoupled	Coupled	Observed
SLP	24	960.1 hPa	958.2 hPa	923 hPa
SLP	48	933.6 hPa	925.7 hPa	910 hPa
U_{max}	24	41.1/62.6 m s^{-1}	36.6/59.9 m s^{-1}	67.0 m s^{-1}
U_{max}	48	52.6/77.0 m s^{-1}	50.1/73.8 m s^{-1}	77.0 m s^{-1}
H_s	24	14.9 m	13.9 m	
H_s	48	17.2 m	15.1 m	
α_{max}	24	0.0185	0.18	
α_{max}	48	0.0185	0.32	

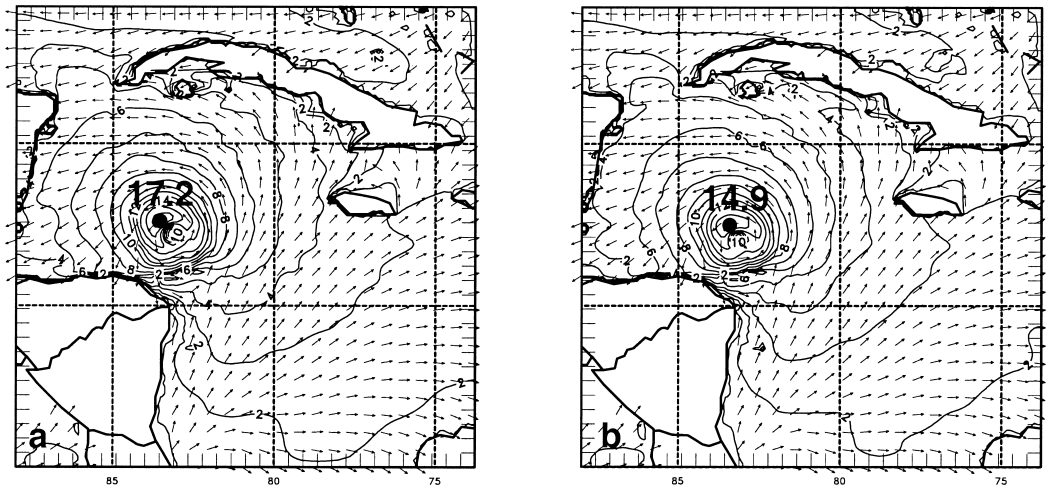

FIG. 10. Significant wave height (m) and direction (vectors) for (a) uncoupled and (b) coupled simulations of Tropical Cyclone Mitch valid at 0000 UTC 27 Oct 1998 (48-h time).

large impact on the spatial character of the ocean wave response. Unfortunately, no observed estimates of the wave fields are available for this time. The Charnock parameter is shown in Fig. 11 for 0000 UTC 26 October. The maximum Charnock parameter is 0.1 at this time, which is nearly an order of magnitude larger than the conventional parameter valid for the open ocean featuring a mature wave state. Also, the Charnock parameter maximum undergoes a threefold increase between 0000 UTC 26 October and 0000 UTC 27 October coinciding with the time period of rapid intensification of the tropical cyclone (i.e., minimum sea level pressure decreases by 27 hPa in the 33-h period in the coupled simulation). It is noteworthy that the Charnock parameter is a maximum near the eyewall structure coincident with the highest wind speeds and a minimum within the eye. Similar to the simulation of Tropical Cyclone Bonnie, the enhanced roughness effects due to the young wave state have a minimal impact on the tropical cyclone track, in spite of the significant changes in the central pressure. For example, at 0000 UTC 27 October (48 h), the position of the tropical cyclone differs by one grid point (12 km) in the two simulations.

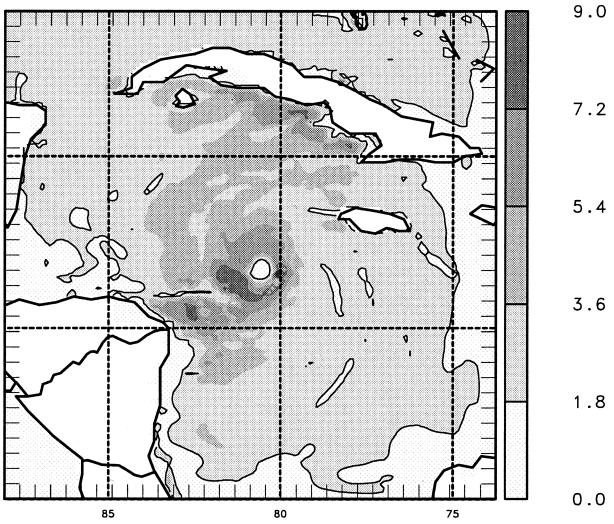

FIG. 11. Charnock parameter ($\times 10^{-2}$) for Tropical Cyclone Mitch valid at 0000 UTC 26 Oct 1998 (24 h) shown by the gray shading scale. The 0.0181 contour is also shown.

c. *Tropical Cyclone Bret simulations*

Tropical Cyclone Bret was an intense hurricane with a relatively small size that formed in the Gulf of Mexico and eventually made landfall along the south Texas coast. Near the time of peak intensity, hurricane force winds were confined to a narrow radius of approximately 50 km wide in the northern portion of the cyclone and 25 km to the south.

The simulated characteristics of the atmospheric and wave fields are summarized in Table 3. The central pressure of the tropical cyclone is approximately 3 hPa lower in the coupled simulation than in the uncoupled case, in slightly better agreement with the estimated values based on in situ observations. The maximum wind speed at 10 and 500 m is once again slightly reduced due to the wave age effects. The significant wave height maximum is approximately 0.5 m lower in the coupled simulation, generally similar to the response of Tropical Cyclones Bonnie and Mitch. One noteworthy aspect of Bret was that the operational NOGAPS had a large track error of over 400 km at 48 h, verifying at 1200 UTC 22 August 1999. The uncoupled and coupled simulations contained a similar error, implying that the track simulation is once again insensitive to any wave coupling issues.

TABLE 3. Same as Table 1, except for Tropical Cyclone Bret valid at 1200 UTC 21 Aug (24 h) and 1200 UTC 22 Aug 1999 (48 h).

Variable	Simulation time (h)	Uncoupled	Coupled	Observed
SLP	24	987.2 hPa	983.9 hPa	979 hPa
SLP	48	955.2 hPa	952.1 hPa	944 hPa
U_{max}	24	30.4/45.7 m s^{-1}	30.5/47.4 m s^{-1}	41.0 m s^{-1}
U_{max}	48	44.1/66.9 m s^{-1}	41.8/66.2 m s^{-1}	64.0 m s^{-1}
H_s	24	8.3 m	7.6 m	
H_s	48	12.3 m	11.8 m	
α_{max}	24	0.0185	0.10	
α_{max}	48	0.0185	0.32	

d. Bora simulations

The Mesoscale Alpine Programme (MAP) took place during fall 1999 with the objective to measure and understand topographically forced moist and dry atmospheric phenomena in the vicinity of the Alps (Bougeault et al. 2001). On 7 November 1999, a severe downslope wind storm occurred in the lee of the Dinirac Alps of Slovenia and Croatia; this type of wind often referred to locally as a bora (Smith 1987). Research aircraft measurements in the low levels indicate wind speeds were in excess of 30 m s^{-1} along the coast at 1.5 km above the Adriatic Sea.

Coupled and uncoupled simulations of the bora were performed using COAMPS with a horizontal grid increment of 5 km. The strong downslope winds in the simulation extended westward over the Adriatic and resulted in a significant enhancement to the surface roughness as a result of the growing waves in the fetch-limited conditions, as shown in Fig. 12a. Plumes of large surface roughness extend across the Adriatic and are associated with the fetch-limited downslope flow. However, in spite of the larger roughness used in the atmospheric model due to the coupled feedback, in general, the simulated atmospheric and wave fields are quite comparable. For example, the wind speed difference at 10 m between the coupled and uncoupled simulations, shown in Fig. 12b, differs by less than 3.0 m s^{-1}, which is comparatively small in relation to the maximum bora speed of 25 m s^{-1} near the surface. Overall the wave coupling appears to have minimal impact on the atmospheric wind and thermal fields. The timescale in this case is likely too short to produce a significant two-way interaction response between the atmosphere and ocean surface waves. This result is in overall qualitative agreement with Janssen and Viterbo (1996) who found that the impact of wave–atmosphere coupling is significant for longer timescale processes, such as those that affect the atmospheric and wave climate.

4. Summary and conclusions

In this study, three tropical cyclones and a topographically forced bora event over the Mediterranean Sea were simulated using a coupled atmosphere–ocean wave model, COAMPS. The model consists of a nonhydrostatic atmospheric model, COAMPS, coupled with a wave model, WAM. The coupled modeling system is capable of enhancing surface stress, due to young ocean

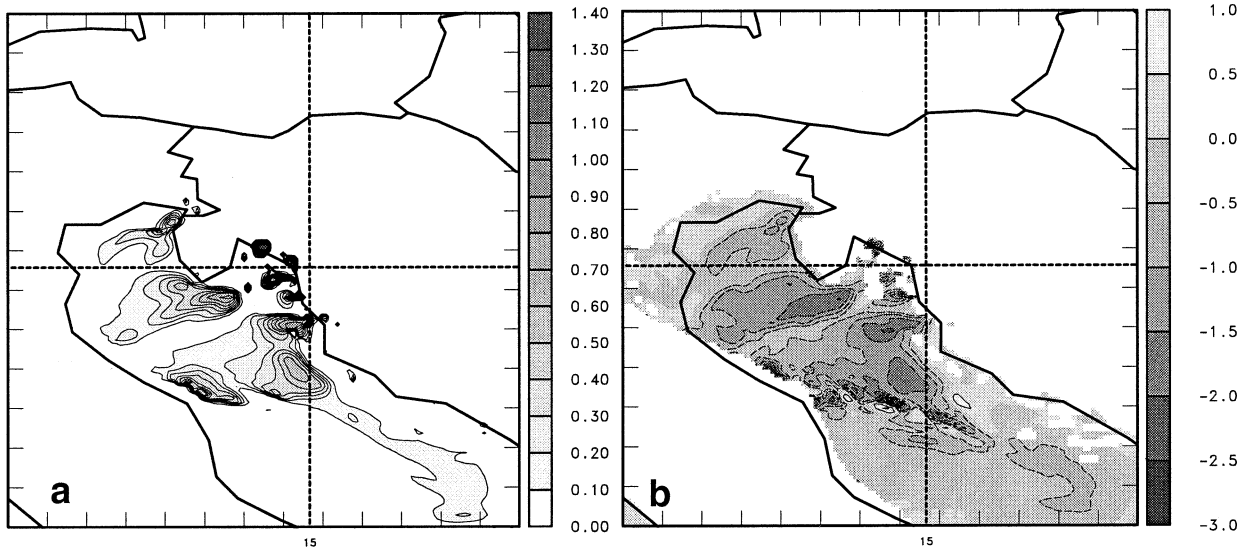

FIG. 12. Simulated (a) roughness length difference (cm) and (b) 10-m wind speed difference (m s^{-1}) between the coupled and uncoupled simulations valid at 1200 UTC 7 Nov 1999 (12 h).

waves in fetch-limited conditions, beyond values yielded by the conventional Charnock scaling relationship. The models were integrated simultaneously and on identical grids with horizontal grid increments ranging from 12 to 5 km. The impact of the wave-induced stress was largest for the strongest of the three tropical cyclones, Mitch. The central pressure in the coupled simulation in this particular case was 8 hPa more intense than the uncoupled simulation due to larger surface heat and moisture fluxes that significantly augmented the precipitation. This intensification apparently resulted primarily from a weak dependence of heat and moisture flux on the wave state. Other tropical cyclone simulations indicated less sensitivity to wave-induced effects. In general, the low-level wind speeds were insensitive to the coupling in spite of a Charnock parameter increase by more than an order of magnitude. Maximum low-level wind speeds typically were 2–3 m s^{-1} less due to the feedback of ocean wave-induced stress. However, local differences in excess of 10 m s^{-1} were found. Significant wave height maxima were reduced by approximately 10% in the coupled simulations due to the enhanced roughness associated with the young ocean waves. The reduced significant wave heights simulated by the coupled model were in closer agreement with the SRA observations for Tropical Cyclone Bonnie than for the uncoupled simulation. The simulated tropical cyclone tracks were insensitive to wave coupling effects. The coupled model indicated reasonable skill in replicating some complex wave spectra characteristics, such as multimodal structures, as observed by SRA for Tropical Cyclone Bonnie. Topographically forced flows in the coastal zone, such as the bora, are characterized by occasionally high near-surface wind speeds and fetch-limited conditions. However, in this study, the bora event was the least sensitive to the ocean-wave-enhanced roughness of all the cases considered. For example, in spite of a substantial increase in the surface roughness associated with the young ocean waves, the near-surface wind speeds differ by less than 3 m s^{-1} between the uncoupled and coupled simulations.

It has become increasingly apparent that surface ocean wave effects due to wave age factors is a key component of the air–sea exchange. Incorporation of surface ocean wave effects into numerical models may be necessary to achieve accurate surface fluxes, particularly in high wind conditions. A number of issues remain unresolved with respect to air–sea interaction in high wind conditions. The accuracy of wind energy transfer, dissipation and nonlinearity representations in wave models, surface flux exchange at the air–sea interface in atmospheric models, and air–ocean coupling methodologies need to be assessed. In the high wind regime in particular, gustiness effects and mesoscale transients need to be considered in order to improve surface wind stress forcing. Finally, an improved representation of the bulk effect of sea spray on the fluxes of heat and moisture may be required before realistic simulations of air–sea interaction at high wind speeds can be achieved.

Acknowledgments. This research was supported by ONR PE0602435N and PE0601153N. Computing time was supported by a grant of HPC time from the DoD HPC MSRCs at Stennis, Mississippi, and Aberdeen, Maryland. Comments from Peter Janssen and two anonymous reviewers substantially improved this manuscript. Benifical discussions with Paul Wittmann and Joao Teixeira also contributed to this study. COAMPS is a trademark of the Naval Research Laboratory.

REFERENCES

Bao, J.-W., J. M. Wilczak, J.-K. Choi, and L. H. Kantha, 2000: Numerical simulations of air–sea interaction under high wind conditions using a coupled model: A study of hurricane development. *Mon. Wea. Rev,* **128,** 2190–2210.

Bougeault, P., and Coauthors, 2001: The MAP special observing period. *Bull. Amer. Meteor. Soc.,* **82,** 433–462.

Charnock, H., 1955: Wind stress on a water surface. *Quart. J. Roy. Meteor. Soc.,* **81,** 639–640.

Desjardins, S., J. Mailhot, and R. Lalbeharry, 2000: Examination of the impact of a coupled atmospheric and ocean wave system. Part I. Atmospheric aspects. *J. Phys. Oceanogr.,* **30,** 385–401.

Donelan, M., 1990: Air–sea interaction. *The Sea,* B. LeMehaute and D. M. Hanes, Eds., Ocean Engineering Science, Vol. 9, Wiley and Sons, 239–292.

Doyle, J. D., 1995: Coupled ocean wave/atmosphere mesoscale model simulations of cyclogenesis. *Tellus,* **47A,** 766–788.

Emanuel, K. A., 1995: Sensitivity of tropical cyclones to surface exchange coefficients and a revised steady-state model incorporating eye dynamics. *J. Atmos. Sci.,* **52,** 3969–3976.

Geernaert, G. L., S. E. Larsen, and F. Hansen, 1987: Measurements of the wind stress, heat flux and turbulence over the ocean. *Global Atmos. Ocean Syst.,* **2,** 121–142.

Hodur, R. M., 1997: The Naval Research Laboratory's Coupled Ocean/Atmosphere Mesoscale Prediction System (COAMPS). *Mon. Wea. Rev.,* **125,** 1414–1430.

——, and J. D. Doyle, 1999: The Coupled Ocean/Atmosphere MesoScale Model Prediction System (COAMPS). *Coastal Ocean Prediction,* C. N. K. Mooers, Ed., Coastal and Estuarine Studies, Vol. 56, Amer. Geophys. Union, 125–155.

Janssen, P. A. E. M., 1989: Wave-induced stress and the drag of air flow over sea waves. *J. Phys. Oceanogr.,* **19,** 745–754.

——, 1991: Quasi-linear theory of wind-wave generation applied to wave forecasting. *J. Phys. Oceanogr.,* **21,** 1631–1642.

——, and P. Viterbo, 1996: Ocean waves and the atmospheric climate. *J. Climate,* **9,** 1269–1287.

——, J. D. Doyle, J. Bidlot, B. Hansen, L. Isaksen, and P. Viterbo, 2002: Impact and feedback of ocean waves on the atmosphere. *Advances in Fluid Dynamics,* Vol. 1, *Atmosphere–Ocean Interactions,* W. Perrie, Ed., WIT Press, 155–198.

Kepert, J. D., C. W. Fairall, and J. W. Bao, 1999: Modelling the interaction between the atmospheric boundary layer and evaporating sea spray droplets. *Air–Sea Fluxes of Momentum, Heat and Chemicals,* G. L. Geeraert, Ed., Kluwer Academic, 363–409.

Kudryavtsev, V. N., and V. K. Makin, 2001: The impact of air-flow separation on the drag of the sea surface. *Bound.-Layer Meteor.,* **98,** 155–171.

Lalbeharry, R., J. Mailhot, S. Desjardins, and L. Wilson, 2000: Examination of the impact of a coupled atmospheric and ocean wave system. Part II: Ocean wave aspects. *J. Phys. Oceanogr.,* **30,** 402–415.

Lionello, P., P. Malguzzi, and A. Buzzi, 1998: Coupling between the

atmospheric circulation and ocean wave field: An idealized case. *J. Phys. Oceanogr.,* **28,** 161–177.

Louis, J. F., M. Tiedtke, and J. F. Geleyn, 1982: A short history of the operational PBL-parameterization at ECMWF. *Proc. Workshop on Planetary Boundary Layer Parameterization,* Reading, United Kingdom, ECMWF, 59–79.

MacAfee, A. W., and P. J. Bowyer, 2000: Trapped-fetch waves in a transitioning tropical cyclone (Part I – The need and theory). Preprints, *24th Conf. on Hurricanes and Tropical Meteorology,* Fort Lauderdale, FL, Amer. Meteor. Soc., 292–293.

Mellor, G. L., and T. Yamada, 1982: Development of a turbulence closure for geophysical fluid problems. *Rev. Geophys. Space Phys.,* **20,** 851–875.

Moon, I., I. Ginis, and T. Hare, 2002: Response of sea surface direction wave spectra in a hurricane to the storm translational speed. *Ocean Sciences Meeting,* Honolulu, HI, Amer. Geophys. Union and American Society of Limnology and Oceanography, OS42B-130.

Oost, W. A., G. J. Komen, C. M. J. Jacobs, C. van Oort, and H. Bonekamp, 2001: Indications for a wave dependent Charnock parameter from measurements during ASGAMAGE. *Geophys. Res. Lett.,* **28,** 2795–2797.

Powers, J. G., and M. T. Stoelinga, 2000: A coupled air–sea mesoscale model: Experiments in atmospheric sensitivity to marine roughness. *Mon. Wea. Rev.,* **128,** 208–228.

Smith, R. B., 1987: Aerial observations of the Yugoslavian bora. *J. Atmos. Sci.,* **44,** 269–297.

Smith, S. D., and Coauthors, 1992: Sea surface wind stress and drag coefficients. The HEXOS results. *Bound.-Layer Meteor.,* **60,** 109–142.

Walsh, E. J., L. K. Shay, H. C. Graber, A. Guillaume, D. Vandemark, D. E. Hines, R. N. Swift, and J. F. Scott, 1996: Observations of surface wave-current interaction during SWADE. *Global Atmos. Ocean Syst.,* **5,** 99–124.

WAMDI Group, 1988: The WAM model—A third-generation ocean wave prediction model. *J. Phys. Oceanogr.,* **18,** 1775–1810.

Wang, Y., J. D. Kepert, and G. J. Holland, 2001: The effect of sea spray evaporation on tropical cyclone boundary layer structure and intensity. *Mon. Wea. Rev.,* **129,** 2481–2500.

Weber, S. L., H. von Storch, P. Viterbo, and L. Zambresky, 1993: Coupling an ocean wave model to an atmospheric general circulation model. *Climate Dyn.,* **9,** 53–61.

Wright, C. W., 2000: Open ocean and landfalling hurricane directional wave spectra from a scanning radar altimeter. *Proc. Sixth Int. Conf. on Remote Sensing for Marine and Coastal Environments,* Charleston, SC, Veridian-ERIM and NOAA/NESDIS, Vol. 1, 9–15.

——, and Coauthors, 2001: Hurricane direction wave spectrum variation in the open ocean. *J. Phys. Oceanogr.,* **31,** 2472–2488.

Young, I. R., 1988: Parametric hurricane wave prediction model. *J. Waterway, Port, Coastal Ocean Eng.,* **114,** 637–652.

Zhang, Y., and W. Perrie, 2001: Feedback mechanisms for the atmosphere and ocean surface. *Bound.-Layer Meteor.,* **100,** 321–348.